Spatio-temporal mode description in LiDAR point clouds

Oliver L. GEISSENDÖRFER[1,*] and **Christoph HOLST**[1]

[1] *Chair of Engineering Geodesy, TUM School of Engineering and Design, Technical University of Munich, Germany, (o.geissendoerfer@tum.de, christoph.holst@tum.de)*

[*] *corresponding author*

Abstract

Analyzing objects concerning their static and dynamic change is mostly performed with IMU (Inertial Measurement Units) or GNSS (Global Navigation Satellite System) sensors fixed to a physically defined surface. We can use a total station to record additional data or support other sensors by referencing them to a homogeneous coordinate frame. LiDAR (Light Detection and Ranging) enables simultaneous, contactless, spatially connected, and time-referenced observations recording an object.
All sensors share the ability to detect equivalent signal properties concerning different signal-to-noise ratios. Since object deformation is not limited to a fixed position, we must continuously model or interpret the dynamic movement within our processing to get a spatio-temporal understanding. Therefore, LiDAR offers advanced options for understanding the spatio-temporal behavior of an object with a frequency analysis executed in the or time domain.
In our work, point clouds are processed in a state-of-the-art time series analysis of discretized locations in the frequency domain. Furthermore, fusing point cloud observations in a time domain approach offers a unique opportunity to analyze the spatio-temporal behavior of objects. This observation-level fusion reduces the number of required processing steps. The resulting parameter model leads to simplification of present periodic signals, yet retaining spatial and temporal consistency and streamlining subsequent interpretation.

Keywords: MEMS-LiDAR, frequency analysis, mode analysis

Received: 20th November 2024. Revised: 13th March 2025. Accepted: 13th March 2025.

1 Introduction

Light detection and ranging (LiDAR) sensors have earned significant attention in recent years due to their ability to provide dense 3D observations. LiDAR is used within monitoring applications such as bridges, skyscrapers, and natural processes to gain insights into their underlying behavioral patterns. Patterns consist of linear trends, irregularities, and dynamic changes. Periodic deformations are analyzed, especially by combining multiple sensors or descriptive targets that symbolize an individual point. Points are observed by sensors like global navigation satellite system (GNSS) (Hohensinn et al., 2020; Schönberger et al., 2023), inertial measurement unit (IMU) (Xiong et al., 2017; Sabato et al., 2017), and Total Stations (TS) (Wagner et al., 2013). Moreover, their spatial distribution substantially impacts the monitoring results as described by Mendler et al. (2022).
Cameras (Chen et al., 2017; Del Sal et al., 2021; Luo et al., 2024) and laser vibrometry (Martarelli et al., 2001; Staszewski et al., 2007; Di Maio et al., 2021; Yu et al., 2024) are approaches used to investigate and monitor the spatial behavior of structures. Compared with GNSS, IMU, and TS setup, cameras, and laser vibrometry remotely observe structures, making them easy to operate and requiring less human interaction with structures when they are at risk. In general, cameras are relatively cheap passive sensors, whereas laser vibrometry represents an active sensor that is more costly to operate. The sensor's nature and operating principle also affect the potential observation range since an adequate illumination is needed for cameras and sensors using a laser source, which depends on the supplied

laser energy. However, they observe defined points in image coordinates or polar coordinates multiple times to create a spectrum at various locations and move to the next position. Thus, observations are connected spatially but are only processed consecutively.
On the other hand, light detection and ranging (LiDAR) sensors also provide contactless observations, whereas points are recorded subsequently in space. Moreover, an object time series is constantly built for all locations on a structure simultaneously, and all observations are commonly referenced in time. Generally, MEMS (Micro-Electro-Mechanical Systems) sensors, particularly 3D MEMS-LiDAR sensors employ a low-cost option to observe structures continuously in space and time.
When detecting deformations in a monitoring setting based on LiDAR, we generally compare individual points, local neighborhoods, or geometric primitives to analyze irreversible or recurring changes between multiple epochs (Raffl and Wunderlich, 2020; Ötsch et al., 2023; Raffl and Holst, 2024). In this work, we investigate dynamic environments and focus on periodic changes by applying an adaptable mathematical model to approximate the immovable mean surface, amplitude, and phase corresponding to multiple frequencies in the time domain.
All parameters determined within a dynamic environment show different relationships in space and time. Furthermore, the behavior within space and in time can be determined for each spatial location individually, or by combining observations directly using spatio-temporal connections. Thus, we answer three research questions within our work:

- Can we determine the spatio-temporal connections of a 3D time series within a frequency analysis in the time domain?
- How does point-wise feature-level processing and observation-level processing in the time domain compare against each other?
- Do observation residuals show systematics after parameter determination?

Investigating different approaches for point cloud time series processing within dynamic environments provides geometric understanding using so-called mode shapes, which depict high frequent deformations of structures. In addition, it reveals new application fields for operational modal analysis identifying cracks and the health of built structures during operation, such as in Yu et al. (2014), but with a continuously observing low-cost MEMS-LiDAR sensor. Therefore, cracks can be identified by changing mode shapes of built structures e.g. bridges or noise barrier walls. Furthermore, we aim to make our methodology more applicable for non-contact LiDAR observations and to complement existing approaches and sensors. Additionally, our methodology solely focuses on a data-driven strategy instead of introducing physics or prior knowledge into the estimation process.

2 Related work

Technological innovations such as more accurate LiDAR observations and the decreasing costs of LiDAR systems, they gained more attention in several fields. The automotive industry also developed low-cost sensors with different characteristics that are applied in various scenarios (Holzhüter et al., 2023). Low-cost MEMS-LiDAR sensors are used to increase robustness in vehicle operation within the sector of autonomous driving (Yoo et al., 2018). However, the quality of a MEMS-LiDAR sensor concerning high-quality LiDAR point clouds and photogrammetric point clouds is shown in Bakuła et al. (2022).
Conducting a frequency analysis on a point cloud time series was first executed by Schill and Eichhorn (2019) as well as Meyer et al. (2023) to detect frequencies induced by a bypassing train using spatial relationships within recorded observations. Processing observation data in space and in time requires a methodological approach using spatio-temporal connections which was conducted in Holst and Neuner (2021). Subsequently, Geißendörfer and Holst (2024) compared different approaches using high-quality profile LiDAR instruments in the time domain determining frequencies and their spatial distribution of an artificial rigid object with forced excitation.
Geißendörfer and Holst (2025) then extend the work to a more flexible object and observe its movement after forced excitation comparing MEMS-LiDAR sensors. The experiment shows a time-domain frequency analysis application concerning 3D point cloud time series. Furthermore, two MEMS-LiDAR sensors are compared while focusing on their scan pattern resulting in a varying resolution capability

and a different ability to process periodic signals.
The described work shows the development of point cloud time series processing with low-cost MEMS-LiDAR sensors. 3D point clouds that are continuous in time enable various applications regarding spatial analysis and frequency determination. Frequency processing of 3D point clouds requires an altered workflow than state-of-the-art frequency analysis techniques (Welch, 1967; Strang, 1994). Therefore, Geißendörfer and Holst (2024) presented different approaches to process 2D point clouds concerning frequency analysis.
We conduct different approaches with 3D point clouds. Approaches are continuous in time determining so-called mode shapes that describe the spatial relationship concerning individual frequencies (Gentile and Bernardini, 2008). Therefore, we compute mode shapes based on a feature- or observation-level approach clearing the path of analyzing geometric variations in the future.

3 Mode shapes from 3D point clouds in time

Low-cost MEMS-LiDAR sensors are a cost-effective alternative to high-end sensors. In our user case investigating the methodology, high-end sensors often only provide time information in a 2D measurement setting. On the other hand, low-cost sensors provide raw data without limiting software policies. These MEMS-LiDARs are limited in their field of view but they record continuous point clouds with a time stamp given to each point individually.

3.1 MEMS-LiDAR

We use the Livox Avia, a 3D MEMS-LiDAR sensor operating a deflective mirror that enables the selection of two distinctive scan patterns. Scan patterns are distinguished by a non-repetitive scan pattern observing its environment at varying locations with a field of view (FOV) of $70.4° \times 77.2°$. In contrast, the repetitive scan pattern repeats its observation location employing a FOV of $70.4° \times 4.5°$ neglecting potential locations on the desired object. Both scan patterns make use of separate lines steered accordingly with predefined directions.

Because of the FOV, we use Livox Avia's non-repetitive scan pattern in Fig. 1 as an information base to avoid limitations resulting from a repetitive scan pattern. The non-repetitive characteristic enables unstructured point observations referenced in time and relatively in space. In addition, the non-repetitive nature causes the fact that we cannot assume point-wise correspondence in time. However, disregarding the scan pattern with its different characteristics, the Livox Avia records up to 240.000 points per second at a maximum distance of 450 meters, making it practicable for many applications. Additionally, the manufacturer gives a range precision of 2 centimeters considering its polar observation principle.

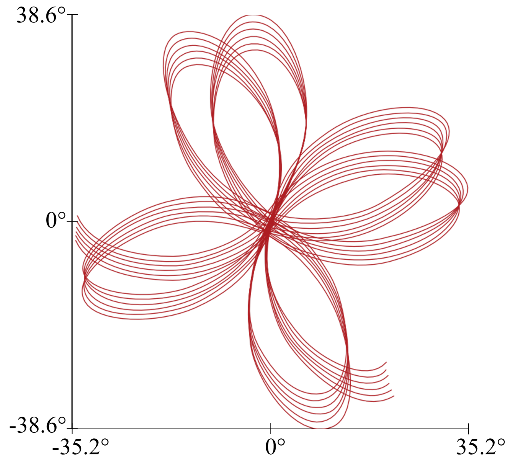

Figure 1. The non-repetitive scan pattern of the Livox Avia. The scan pattern rotates anti-clockwise by time to cover the full field of view, 70.4° (horizontally) and 77.2° (vertically). With this unique scan-pattern, it densifies the point cloud by time.

Using MEMS-LiDAR sensors enables simultaneous and continuous observations of physical objects within a limited FOV making multiple sensors for these spatial areas obsolete. However, the low-cost sensor heritage produces a low signal-to-noise ratio (SNR). Moreover, the Livox Avia shows some outshining of the receiving unit when objects are close and are located in the center of the FOV corrupting observations as shown in our setup in Fig. 2.

3.2 Experimental setup and pre-processing

3D MEMS-LiDAR sensors give geometric and timely observations as a point cloud time series for frequency analysis. Within the frequency analysis context, we determine the periodic signals and aim to describe their spatial distribution concerning the

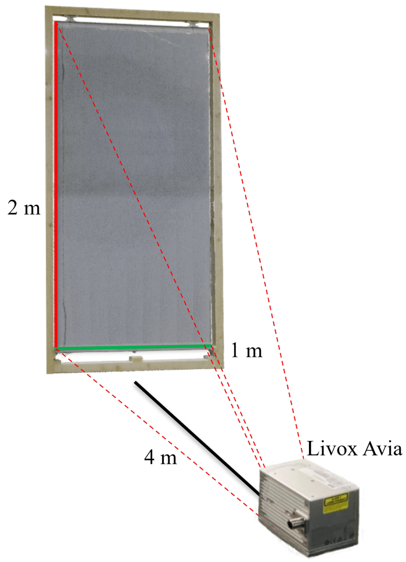

Figure 2. Experimental setup visualizing the acrylic glass sheet and the location of the MEMS-LiDAR sensor recording the object and the movement three-dimensionally.

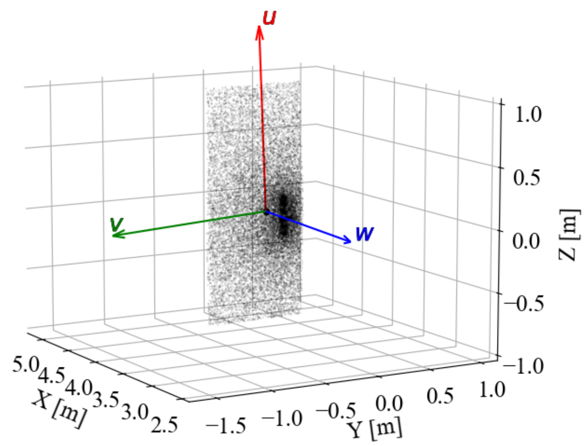

Figure 3. Experimental setup observed by the MEMS-LiDAR sensor along the principal components calculated in the pre-processing. Moreover, the density of observations implicitly visualizes the center of the field of view.

experimental object, called mode shapes. The experimental object is chosen as a non-rigid acrylic glass sheet allowing the impact of external forces.
In our work, we use the forced excitation of the acrylic glass sheet fixed with a dynamic magnitude of ± 30 millimeters and a curved mean. The excitation is actively created by a motor moving the acrylic glass sheet with a linear actuator at a predetermined constant amplitude. In contrast, a constant electric supply sets the main frequency of 0.32 Hertz. Furthermore, the excitation is spatially limited and only given at zero height within Fig. 3. We observe the inducted movement at 4 meters distance, visualized in Fig. 2 allowing an observation-rich coverage of the object.

After recording a point cloud time series with constant amplitude and frequency, we introduce spatial limitations by manually cutting the point cloud to our experimental setup. Moreover, we need to align the periodic movement with a coordinate axis for the shape estimation using principal components (Pearson, 1901) shown in Fig. 3. The alignment regarding the object of investigation results in a coordinate system that minimizes movements within two coordinate axes focusing the forced movement to the third axis.

3.3 Determination of mode shapes

This section compares two approaches calculating mode shapes using a feature- and observation-level approach. To compute the mode shape of frequencies for a spatially limited time series, we apply a binning algorithm to a 3D point cloud. Binning point clouds is a rasterization executed with predefined boundaries in the metric space. Boundaries can be set in the euclidean or polar space. In this work, we chose the euclidean space after aligning the object along its main extension and focusing the movement on the vertical axis avoiding artifacts introduced by the sensor setup location.
When binning a 3D point cloud, we separate observations spatially and assume independent time series. Computing the amplitude within each spatially limited time series as a feature, we must calculate the spatial relationship in a secondary processing step using interpolation. On the other hand, we can directly compute the spatial mode shape using all observations made available by MEMS-LiDAR point clouds. The direct estimation of the mode shape in a time domain least-squares model requires implicit geometric modeling with polynomial surfaces or Non-uniform-rational B-Splines (NURBS) (Piegl and Tiller, 2012).

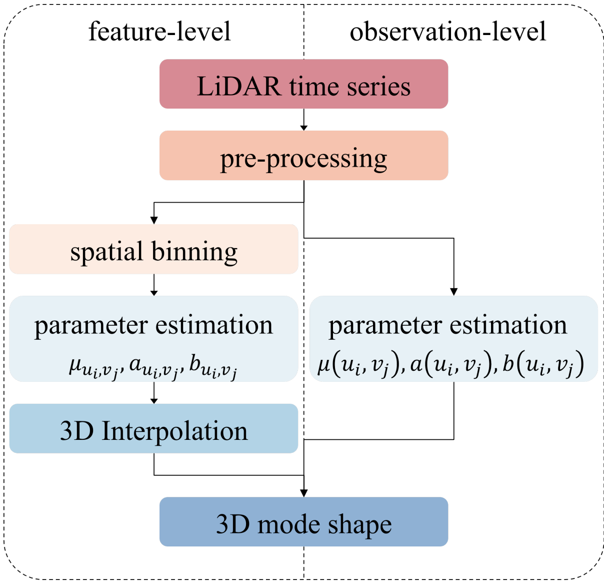

Figure 4. Working steps required to process point clouds in space and time. On the left, we display working steps in a feature-level processing, whereas on the right we skip individual steps since they are obsolete in an observation-level approach.

To compare these two time-domain estimation approaches in Fig. 4, we describe a feature-level approach requiring multiple steps within section 3.3.1, and compare it to observation-level processing in section 3.3.2. We use equivalent frequency starting values in both sections since they are the bottleneck within time domain frequency analysis. Therefore, we fix a pre-defined frequency value f to 0.249 Hz determined with state-of-the-art methods in the field of frequency analysis.

3.3.1 Feature-level processing

Sensors used in vibration monitoring must be placed on the object's surface (Mendler et al., 2022) or remotely observe a point multiple times (Siringoringo and Fujino, 2009). To imitate this behavior, Geißendörfer and Holst (2024) execute a binning of profile LiDAR observations with a constant step width. With 3D MEMS-LiDAR data, we define a raster with a grid size of 50 millimeters along the first and second principal components.
We chose this specific size because of two reasons. First, we ensure that every cell contains points and therefore information. With an observation length of two minutes and an average point density of 8.000 per cell, we end up with an approximate sampling rate of 15 Hz. Due to the non-repetitive scan pattern, some areas stay weakly staffed resulting in a low observation rate whereas in the center of the FOV we can reach up to 170 Hz sampling rate enabling the observation of high frequencies. Secondly, it approximates the size of a mounting that secures other sensors to structures. Thus, keeping the area of impact alike and therefore allows drawing conclusions or comparisons more easily.
Rasterized observations are now used to compute a set of Fourier parameters per grid cell according to

$$\begin{aligned} F(u_i, v_j, t_k) = & \\ & \mu_{u_i,v_j} + \\ & a_{u_i,v_j} \cdot cos(2\pi f t_k) + \\ & b_{u_i,v_j} \cdot sin(2\pi f t_k). \end{aligned} \tag{1}$$

With this distinct description of a single frequency, we characterize the underlying mean $\mu_{i,j}$ with one value to enforce a zero-mean time series. Additionally, Fourier parameters $a_{i,j}$ and $b_{i,j}$ describe the periodic movement with frequency f in its spatial bin. Moreover, we implicitly determine the amplitude and phase information with Fourier parameters at this location. Simultaneously, residuals are computed within each cell to give insights about their distribution. In a second processing step, we apply a cubic spline-based interpolation to map amplitudes and residuals to a geometric surface.
Fig. 5 (a) displays a mode shape interpolated to a surface with an unsymmetric distribution of residuals. Additionally, a color value presents a signed mean residual per grid cell illustrating a tendency of model over- or underestimation concerning the movement's magnitude. However, the magnitude of mean residuals stays mostly constant with an absolute mean of 2.8 millimeters.
Generally, the processing approach generalizes insufficiently in non-continuous locations due to the dependence on the size of raster cells. Thus, the functional model does not adapt well to geometric changes within large cells, whereas the small size of cells risks a low number of points or even staying unoccupied and empty making a frequency analysis impossible. To increase flexibility within a least-squares estimation within equation (1), we must introduce adjustable cell sizes depending on factors like the number of observations, location in the field of view, or object-wise correspondences.

3.3.2 Observation-level processing

With a LiDAR sensor, we generally record relative spatial relationships between points with distance and angle observations. Using a MEMS-LiDAR sensor, angle observations are generated from electronically steered mirrors. Electrical steering of mirrors also impacts the SNR, thus a point-wise comparison is limited because points are not located in the exact same position. Therefore, we can directly model an object's periodic movement by introducing spatio-temporal connections

$$
\begin{aligned}
F(u_i, v_j, t_k) = \\
&\mu(u_i, v_j) + \\
&a(u_i, v_j) \cdot cos(2\pi f t_k) + \\
&b(u_i, v_j) \cdot sin(2\pi f t_k)
\end{aligned}
\tag{2}
$$

as presented in Geißendörfer and Holst (2025). Spatio-temporal connections enforce dependencies in space and time by modeling the mean $\mu(u_i, v_j)$ as well as Fourier parameters $a(u_i, v_j)$ and $b(u_i, v_j)$ according to geometric surfaces. Therefore, the model automatically employs the identical frequency at all spatial locations and enforces implicit spatial relationships. Fig. 5 (b) visualizes the mode shape of an estimated NURBS surface.

Along with its continuous shape and magnitude, we binned the signed mean residuals to the same spatial boundaries of section 3.3.1 to directly compare it to residuals shown in Fig. 5 (a). This binning again fails to see local changes smaller than the bin size of 50 millimeters. Moreover, the magnitude of residuals is mostly constant at ± 3.0 millimeters. Generalizing observations with NURBS will adapt to local geometric artifacts but highly depends on the choice of hyperparameters, such as the structure of knot vectors along principal components or the degree used to create a surface.

4 Discussion

This section will further discuss differences between a feature-level and observation-level frequency analysis starting with pre-processing steps. Additionally, we will have an extensive view of sensor artifacts of MEMS-LiDAR sensors that affect the periodic signal estimation in time-domain approaches. Moreover, we look into potential geometric improvements and future research demands.

First, we compare the pre-processing steps required especially the increased number of steps within the feature-level processing. Therefore, we need to decide on a spatial bin size to include enough points for the subsequent estimation process and consider local geometric variations as well as the impact of noise. Within the observation-level estimation, all MEMS-LiDAR recordings are simultaneously integrated into the observation process. In contrast to the bin size in feature-level processing, we decide on a set of knot vectors along the first and second principal components as hyperparameters.

The selection of knot vectors is as dependent on the local, and global geometric variation as the described feature-level approach. However, NURBS require fewer parameters potentially ignoring areas with low or no geometric change. Well-known algorithms improve and determine NURBS knot vectors such as Gálvez and Iglesias (2011), Gálvez and Iglesias (2013), Iglesias et al. (2015) and Harmening and Neuner (2016).

Secondly, we determine frequency starting values for an adjustment with models stated in equation (1), and equation (2). For time series with a limited spatial extent, we can assume point-wise observations, and perhaps even a regular sampling rate to use well-known approaches such as Welch (1967), or Shensa et al. (1992). Utilizing unstructured point cloud time series, we are limited to a time-domain frequency search. Thus, this work ensures consistency comparing feature-level and observation-level estimation in 3.3.1 and 3.3.2 since requirements are equivalent and identical values are used before the adjustment.

MEMS-LiDAR sensors operate in the low-cost sector. Therefore, observations are affected by a low SNR which impacts the frequency identification and the mean shape as well as the mode shape description. The mean shape approximates the static behavior of an object including sensor artifacts. Thus, we see an outshining of the sensor in Fig. 6 (a) due to a strong reflection in the sensor's center and its decreasing distance quality at this specific location. However, the mean shape also shows a general curvature caused by the vertical erection of our acrylic glass sheet reacting to gravity and its fixation.

A feature-level approach will be affected most since it has a non-existent spatial relationship between bins during the estimation process. On the other hand, an observation-level approach is more prone to the sensor's outshining effect depending on the choice of knot vectors. Moreover, increasing the

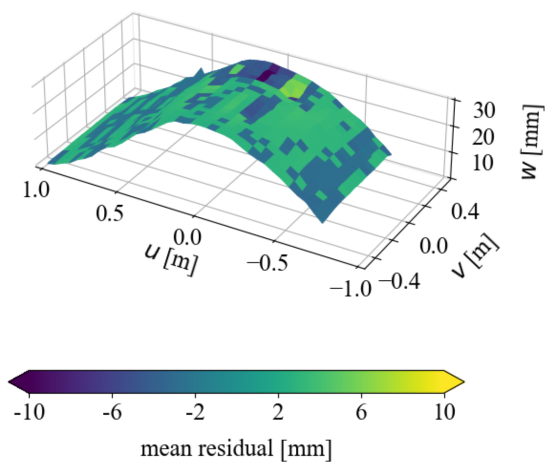

(a) Mode shape corresponding to the amplitude of the dominant frequency combined with the signed mean residuals as a color in the feature-level frequency analysis.

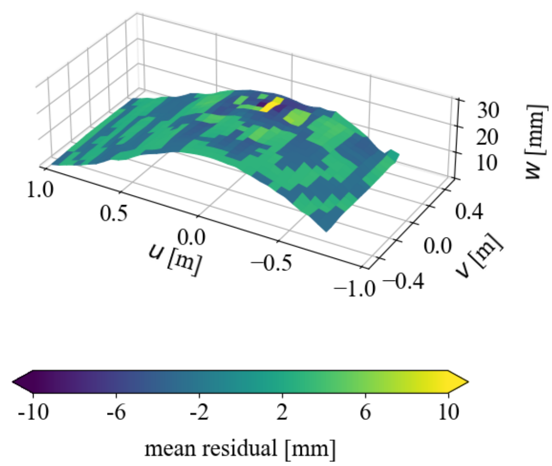

(b) MEMS-LiDAR observations jointly processed across an object by applying NURBS surfaces determining the mode shape of the dominant amplitude on an observation-level along signed mean residuals.

Figure 5. Comparing feature-level and observation-level estimation of the mode shape concerning the dominant frequency. Moreover, the cell size of displayed signed mean residuals for each time series corresponds to a spatial boundary equivalent to 50 millimeters in section 3.3.1.

number of segments within the knot vector makes the geometric mean shape more susceptible to these sensor artifacts. However, mean shapes differ only on a sub-millimeter magnitude when disregarding sensor artifacts.

Besides the mean shape, the mode shape is further highlighted in Fig. 6 (b) describing the amplitude shape of the most dominant frequency. Differences between mode shapes reach a magnitude of 10 millimeters in the middle of the acrylic glass sheet comparing the feature-level and observation-level approach. Moreover, a deviation between approaches diminishes when the magnitude of the forced movement decreases towards the upper and lower object boundary. However, the mode shape is less affected by sensor artifacts resulting in a smooth geometric distribution for both approaches.

Looking at residuals displayed in Fig. 5 (a) and (b), we suspect a contradicting behavior for discussed approaches. The feature-level approach from section 3.3.1 consistently overestimates the mode shape resulting in a negative sign with most residuals within Fig. 5 (a). On the other hand, the observation-level approach within section 3.3.2 seems to underestimate amplitudes specifically in the object's center location where the sensor's outshining takes place.

An underestimation keeps the majority of residuals positive in Fig. 5 (b) pointing out that observations show greater movement than an estimated geometric surface. Nevertheless, approaches provide the same magnitude of residuals with a difference in the submillimeter range.

5 Conclusion

In our work, we discussed both a feature-level approach and an observation-level approach for spatio-temporal mode description in a time-domain frequency analysis setting. Both approaches are based on data recorded by the Livox Avia sensor that provides point observations in 3D space and time. Approaches differ by including spatio-temporal connections in the estimation process in an observation-level solution or applying a two-step process on a feature-level.

Residuals do not distribute equivalently for presented approaches. Thus, we see the feature-level processing overestimating the mode shape, whereas the observation-level approach underestimates the magnitude. On the other hand, the mean shape is most affected by sensor artifacts in both cases, whereas the observation-level approach minimizes

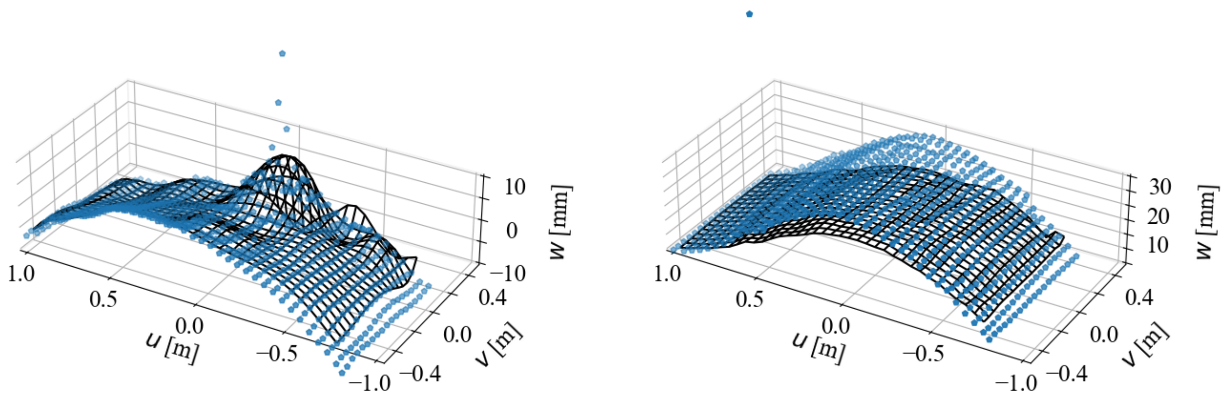

(a) Mean shape comparing the feature-level as point-wise features and the observation-level estimation as a continuous surface. Both are affected by static sensor artifacts.

(b) Mode shape of the dominant mode with a 0.249 Hz frequency. Comparing the feature-level approach as individual point sources with the observation-level estimation.

Figure 6. Comparison of the estimation results including the mean shape and the mode shape corresponding to most the dominant frequency. The feature-level estimation is depicted as 3D points, whereas the observation-level mode determination using NURBS is displayed as a continuous geometric surface.

its influence. Disregarding sensor artifacts, residuals stay on the same level considering the absolute mean residual value.

However, both approaches require hyperparameters to be set. The feature-level approach needs a selection of bin sizes, whereas a small bin size risks noisy or no estimation results at some locations. Processing on an observation-level only considering object limitations, introduces a model selection problem. In this work, we decide to use NURBS modeling Fourier parameters. Therefore, knot vectors with knot locations and the corresponding degree need to be selected.

Furthermore, a careful determination of frequency starting values is indispensable. Taking into account the unstructured and non-uniform distribution of time stamps, we have to fall back on time-domain methods computing a reliable spectrum. However, the frequency starting value only poses an approximate value before optimizing the least squares of models (1) and (2).

After analyzing our experimental results, geometric hyperparameters representing Fourier parameters and frequency starting values still require extensive research to enable an automatic time-domain workflow without human intervention. This innovative approach offers an automatic mode description in the future to improve applications in structural health monitoring.

Especially in the field of crack detection, our approach can contribute by defining spatial relationships concerning individual frequencies. Furthermore, the dynamic reduction of sensor artifacts would impact the frequency analysis of the structures in operation. In addition, we use low-cost MEMS-LiDAR, which extends their use case despite its low SNR.

Funding

This research was funded by German Research Foundation (DFG) under grant number 536704264, project "Processing models for analyzing the 3D vibration response of structures using terrestrial laser scanners (PROVILAS)"

References

Bakuła, K., Lejzerowicz, A., Pilarska-Mazurek, M., Ostrowski, W., Górka, J., Biernat, P., Czernic, P., Załęgowski, K., Kleszczewska, K., Węzka, K., Gąsiewski, M., Dmowski, H., and Styś, N. (2022). Sensor Integration and Application of Low-Sized Mobile Mapping Platform Equipped with LIDAR, Gpr and Photogrammetric Sensors. *ISPRS - International Archives of the Photogrammetry, Remote Sensing and Spatial Information Sciences*, 43B1:167–172.

Chen, J. G., Davis, A., Wadhwa, N., Durand, F., Freeman, W. T., and Büyüköztürk, O. (2017). Video camera–based vibration measurement for civil infrastructure applications. *Journal of Infrastructure Systems*, 23(3):B4016013.

Del Sal, R., Dal Bo, L., Turco, E., Fusiello, A., Zanarini, A., Rinaldo, R., and Gardonio, P. (2021). Structural vibration measurement with multiple synchronous cameras. *Mechanical Systems and Signal Processing*, 157:107742.

Di Maio, D., Castellini, P., Martarelli, M., Rothberg, S., Allen, M., Zhu, W., and Ewins, D. (2021). Continuous scanning laser vibrometry: A raison d'être and applications to vibration measurements. *Mechanical Systems and Signal Processing*, 156:107573.

Geißendörfer, O. L. and Holst, C. (2024). Combining LiDAR and Time-Domain Frequency Analysis for Enhanced Spatial Understanding of Vibration Responses. *IEEE Open Journal of Instrumentation and Measurement*, 3:1–14.

Geißendörfer, O. L. and Holst, C. (2025). Mems lidar sensors for low-cost 3d frequency detection. *IEEE Transactions on Instrumentation and Measurement*, 0.

Gentile, C. and Bernardini, G. (2008). Output-only modal identification of a reinforced concrete bridge from radar-based measurements. *NDT & E International*, 41(7):544–553.

Gálvez, A. and Iglesias, A. (2011). Efficient particle swarm optimization approach for data fitting with free knot b-splines. *Computer-Aided Design*, 43(12):1683–1692.

Gálvez, A. and Iglesias, A. (2013). Firefly algorithm for polynomial bézier surface parameterization. *Journal of Applied Mathematics*, 2013(1):237984.

Harmening, C. and Neuner, H. (2016). Choosing the optimal number of b-spline control points (part 1: Methodology and approximation of curves). *Journal of Applied Geodesy*, 10(3):139–157.

Hohensinn, R., Häberling, S., and Geiger, A. (2020). Dynamic displacements from high-rate GNSS: Error modeling and vibration detection. *Measurement*, 157.

Holst, C. and Neuner, H. (2021). Spatio-temporal models for vibration monitoring of elongated structures using profile laser scans. *Remote Sensing*, 13(7).

Holzhüter, H., Bödewadt, J., Bayesteh, S., Aschinger, A., and Blume, H. (2023). Technical concepts of automotive LiDAR sensors: a review. *Optical Engineering*, 62(3):031213.

Iglesias, A., Gálvez, A., and Collantes, M. (2015). Bat algorithm for curve parameterization in data fitting with polynomial bézier curves. In *2015 International Conference on Cyberworlds (CW)*, pages 107–114.

Luo, K., Kong, X., Li, J., Hu, J., and Deng, L. (2024). Motion magnification for video-based vibration measurement of civil structures: A review. *Mechanical Systems and Signal Processing*, 220:111681.

Martarelli, M., Revel, G. M., and Santolini, C. (2001). Automated modal analysis by scanning laser vibrometry: Problems and uncertainties associated with the scanning system calibration. *Mechanical Systems and Signal Processing*, 15(3):581–601.

Mendler, A., Döhler, M., and Ventura, C. E. (2022). Sensor placement with optimal damage detectability for statistical damage detection. *Mechanical Systems and Signal Processing*, 170:108767.

Meyer, N., Schmid, L., Wieser, A., and Medic, T. (2023). Vibration monitoring of a bridge using 2D profile laser scanning: Lessons learned from the comparison of two spatio-temporal processing strategies. In *Proceedings of the 5th Joint International Symposium on Deformation Monitoring - JISDM 2022*, pages 177 – 184, València. Editorial de la Universitat Politècnica de València.

Ötsch, E., Harmening, C., and Neuner, H. (2023). Investigation of space-continuous deformation from point clouds of structured surfaces. *Journal of Applied Geodesy*, 17(2):151–160.

Pearson, K. (1901). Principal components analysis. *The London, Edinburgh, and Dublin Philosophical Magazine and Journal of Science*, 6(2):559.

Piegl, L. and Tiller, W. (2012). *The NURBS book*. Springer Science & Business Media.

Raffl, L. and Holst, C. (2024). Extending geodetic networks for geo-monitoring by supervised point cloud matching. *Journal of Applied Geodesy*.

Raffl, L. and Wunderlich, T. (2020). Challenges and hybrid approaches in alpine rockslide prevention–an alarming case study. *INGEO&SIG 2020*, page 129.

Sabato, A., Niezrecki, C., and Fortino, G. (2017). Wireless MEMS-Based Accelerometer Sensor Boards for Structural Vibration Monitoring: A Review. *IEEE Sensors Journal*, 17(2):226–235.

Schill, F. and Eichhorn, A. (2019). Deformation Monitoring of Railway Bridges with a Profile Laser Scanner. *ZFV Z. Geodäsie Geoinf. Landmanag*, 2:109–118.

Schönberger, C., Lienhart, W., and Kaden, B. (2023). Static and dynamic structural monitoring of civil infrastructure objects with gnss.

Shensa, M. J. et al. (1992). The discrete wavelet transform: wedding the a trous and Mallat algorithms. *IEEE Transactions on signal processing*, 40(10):2464–2482.

Siringoringo, D. M. and Fujino, Y. (2009). Noncontact Operational Modal Analysis of Structural Members by Laser Doppler Vibrometer. *Computer-Aided Civil and Infrastructure Engineering*, 24(4):249–265.

Staszewski, W. J., Lee, B. C., and Traynor, R. (2007). Fatigue crack detection in metallic structures with lamb waves and 3d laser vibrometry. *Measurement Science and Technology*, 18(3):727.

Strang, G. (1994). Wavelets. *American Scientist*, 82(3):250–255.

Wagner, A., Wasmeier, P., Reith, C., and Wunderlich, T. (2013). Bridge monitoring by means of video-tacheometer – a case study. *avn - Allgemeine Vermessungs-Nachrichten*, 120(8-9):283–292.

Welch, P. (1967). The use of fast Fourier transform for the estimation of power spectra: A method based on time averaging over short, modified periodograms. *IEEE Transactions on Audio and Electroacoustics*, 15(2):70–73.

Xiong, C., Lu, H., and Zhu, J. (2017). Operational Modal Analysis of Bridge Structures with Data from GNSS/Accelerometer Measurements. *Sensors*, 17(3).

Yoo, H., Druml, N., Brunner, D., Schwarzl, C., Thurner, T., Hennecke, M., and Schitter, G. (2018). Mems-based lidar for autonomous driving. *Elektrotechnik und Informationstechnik*, 135.2018(October):408–415. Publisher Copyright: © 2018, The Author(s).

Yu, J., Meng, X., Shao, X., Yan, B., and Yang, L. (2014). Identification of dynamic displacements and modal frequencies of a medium-span suspension bridge using multimode gnss processing. *Engineering Structures*, 81:432–443.

Yu, T., Tang, Q., and Vinayaka, S. (2024). Identifying structural properties of a steel railway bridge for structural health monitoring using laser doppler vibrometry. *Automation in Construction*, 160:105320.